Structure, Volume *24*

Supplemental Information

The Y9P Variant of the Titin I27 Module: Structural Determinants of Its Revisited Nanomechanics

Javier Oroz, Marta Bruix, Douglas V. Laurents, Albert Galera-Prat, Jörg Schönfelder, Francisco Javier Cañada, and Mariano Carrión-Vázquez

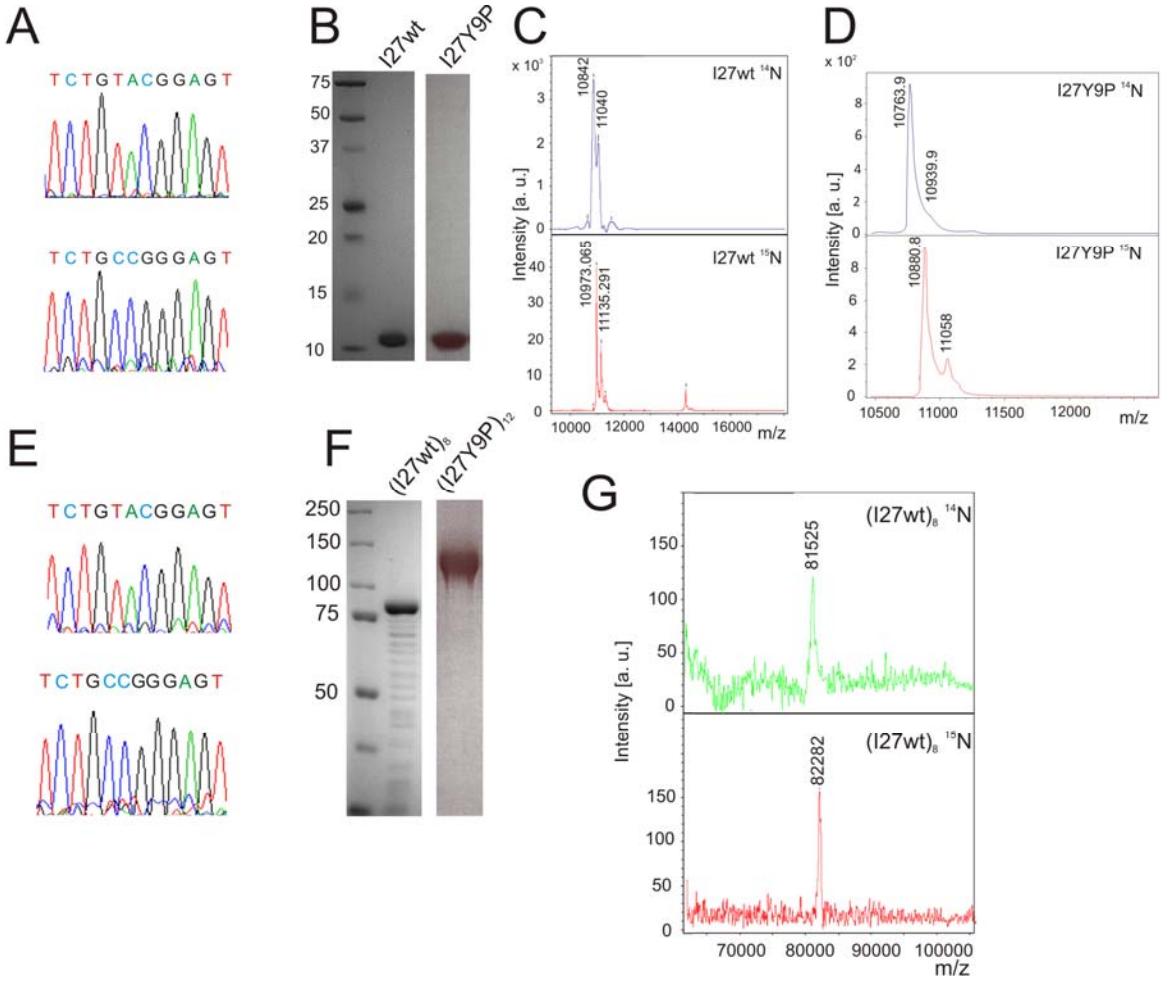

Figure S1. Related to Figures 1, 2, S2, S3 and S4. ^{15}N-labelling for NMR spectroscopy. A) Sequencing chromatograms for I27wt (top) and I27 Y9P (bottom) monomers. The sequence detail shown here verifies the Y9P substitution (TAC→CCG). **B)** ^{15}N-labelled I27wt and I27 Y9P monomers observed in Coomassie Blue-stained 15% SDS-PAGE. According to ProtParam (http://www.expasy.org/tools/protparam.html), both proteins have a nominal size of 11 kDa. **C-D)** MALDI-TOF spectra for ^{14}N and ^{15}N-labelled I27wt (**C**) and I27Y9P monomers (**D**). The ^{15}N incorporation was 97% and 87% in I27wt and I27Y9P, respectively. Both molecules contain a total of 135 nitrogen atoms, and the mass corresponding to full isotopic enrichment was calculated by an increase of 0.996 Da per nitrogen atom in the protein. Whereas the extra peak observed in the I27wt spectra is of unknown origin, the extra peak observed in the I27Y9P spectra (with an increase of ~177 Da) could be due to the typical α-N-6-Phosphogluconoylation of His-tagged proteins that occurs in *E. coli* (Geoghegan et al., 1999). **E)** Sequencing chromatograms for $(I27wt)_8$ (top) and $(I27Y9P)_{12}$ (bottom), showing the TAC→CCG substitution. Both sequences were taken from random repeats in the polyprotein. **F)** Purified ^{15}N $(I27wt)_8$ and $(I27Y9P)_{12}$ observed in Coomassie-Blue stained 8% SDS-PAGE. According to ProtParam, nominal sizes are 82 kDa for $(I27wt)_8$ and 121 kDa for $(I27Y9P)_{12}$. **G)** MALDI-TOF spectra for ^{14}N and ^{15}N-labelled $(I27wt)_8$ revealing 78% ^{15}N incorporation in the latter. $(I27wt)_8$ contains 973 nitrogen atoms. It was not possible to quantify ^{15}N incorporation in $(I27Y9P)_{12}$ in MALDI-TOF due to its large size (> 100 kDa).

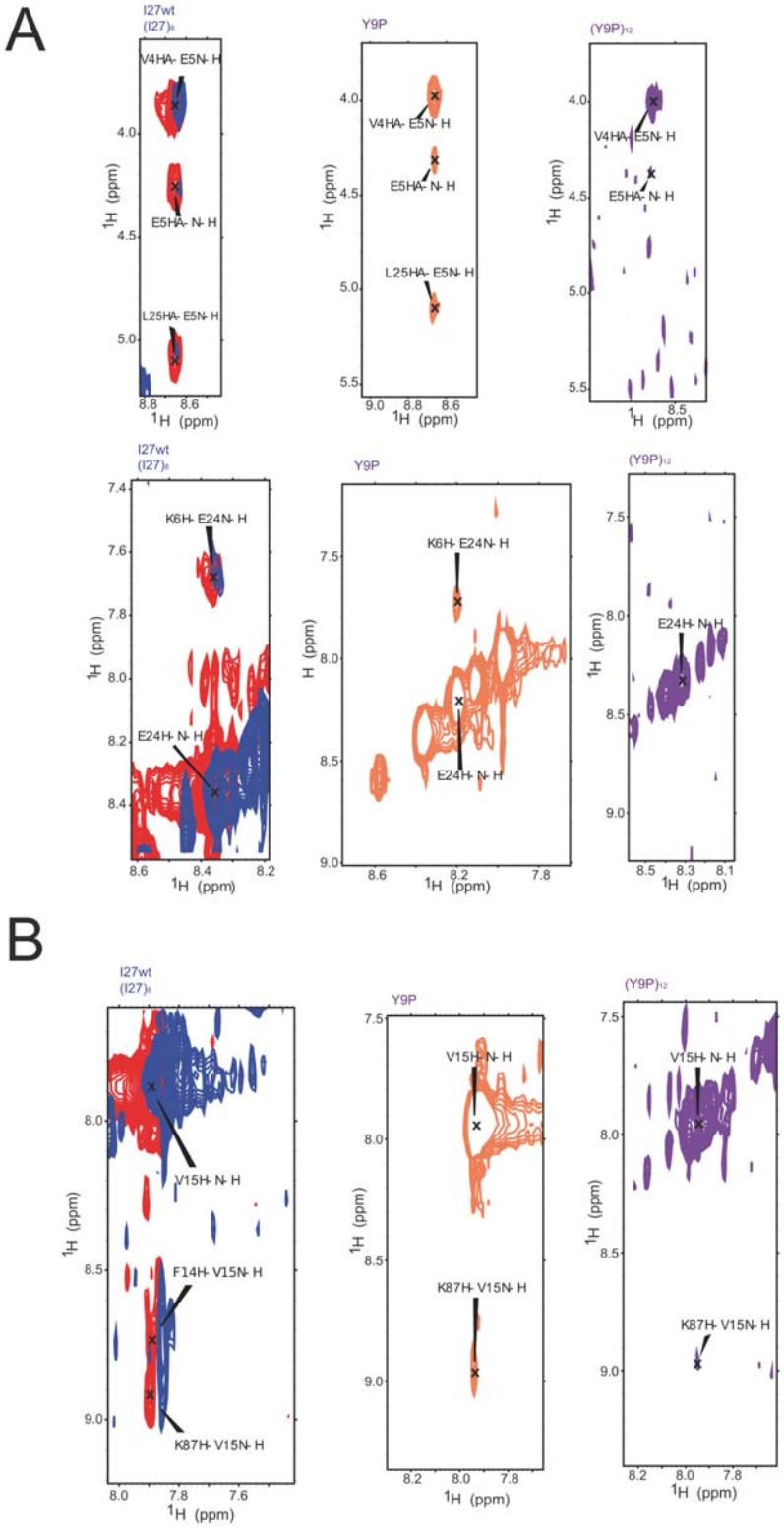

Figure S2. Related to Figure 2. Representative NOEs from residues located in the A-B (mechanical intermediate, A) and A'-G (mechanical clamp, B) patches. Whereas the same NOEs were found in I27wt (red), $(I27wt)_8$ (blue) and I27Y9P (orange), the lack of NOEs between the residues contained in the A-B patch in $(I27Y9P)_{12}$ (**A**, right, in purple) indicate a structural rearrangement in this region leading to the modification of this patch. The NOEs observed between residues contained in the A'-G patch (**B**) are maintained in $(I27Y9P)_{12}$ indicating that this region is not affected. Thus this data perfectly correlate with the lack of mechanical intermediate but identical F_u observed for $(I27Y9P)_{12}$. The spectra corresponding to $(I27wt)_8$ (blue) is intentionally upfield shifted in ^{1}H dimension for clarity.

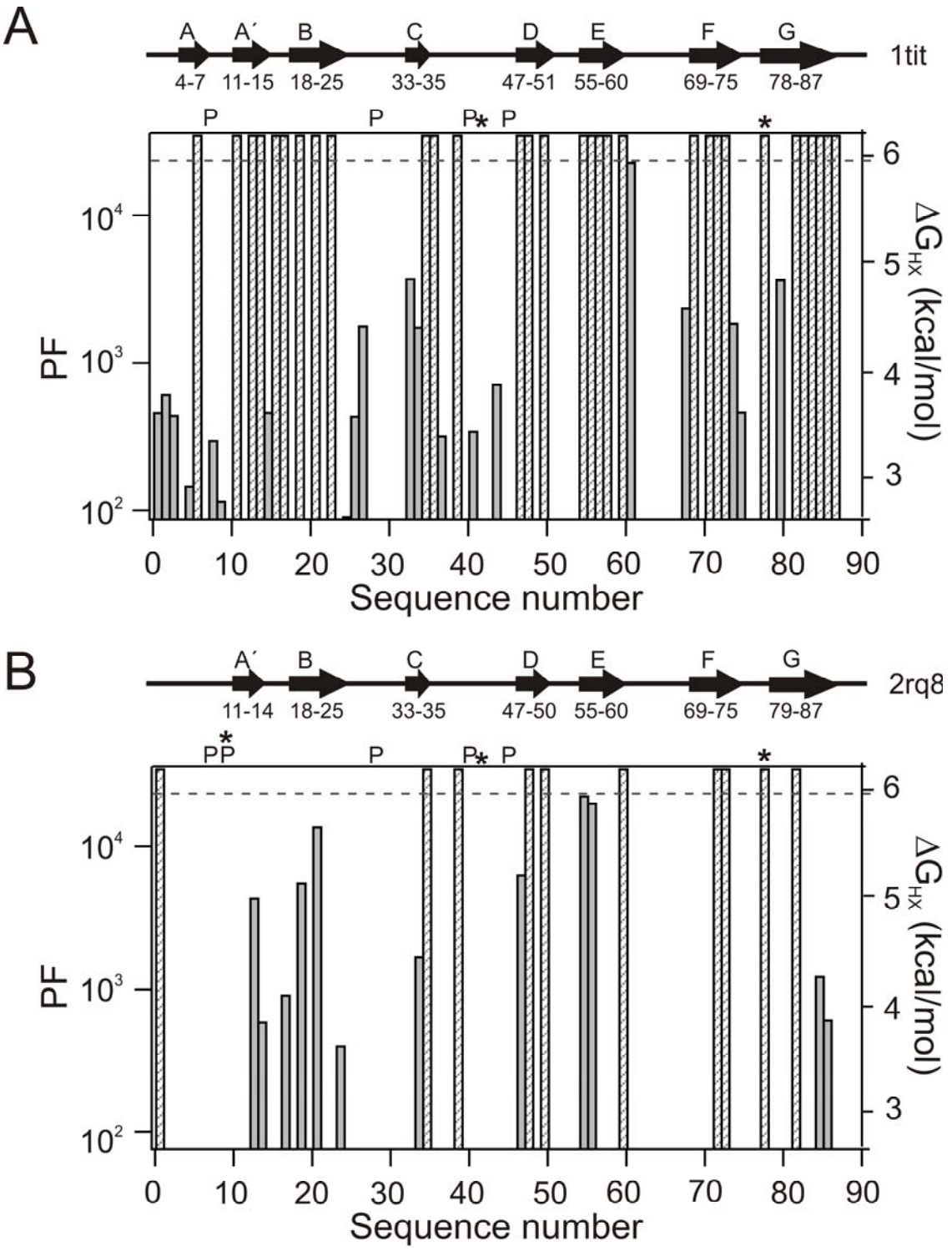

Figure S3. Related to Figure 2. Polyprotein conformational free energy measured by H/D exchange. In both panels, strongly protected HNs that exchange incompletely with solvent deuterons are shown in grey hashed bars, and no bars are shown for HN groups whose exchange is complete in the experimental dead time. **A)** $(I27wt)_8$ amide proton PF values (left axis) and conformational free energy (right). The grey horizontal dotted line shows the highest PF value measured in our experiments, corresponding to H61 ($PF = 2.3 \cdot 10^4$; $\Delta G_{HX} = 5.95$ kcal/mol). The most protected residues ($\Delta G_{HX} > 6$ kcal/mol) correlate with I27wt β-strands, represented as arrows at the top of the panel. P means proline, and the asterisks indicate the substitutions compared to 1tit. **B)** $(I27Y9P)_{12}$ conformational free energy. The exchange of many HNs is faster in $(I27Y9P)_{12}$ than in $(I27wt)_8$, indicating that $(I27Y9P)_{12}$ is less conformationally stable. As explained in **Supplemental Information**, due to a longer dead time before the first spectra was acquired for $(I27Y9P)_{12}$ only H-N crosspeaks signals corresponding to more protected HNs could be monitored.

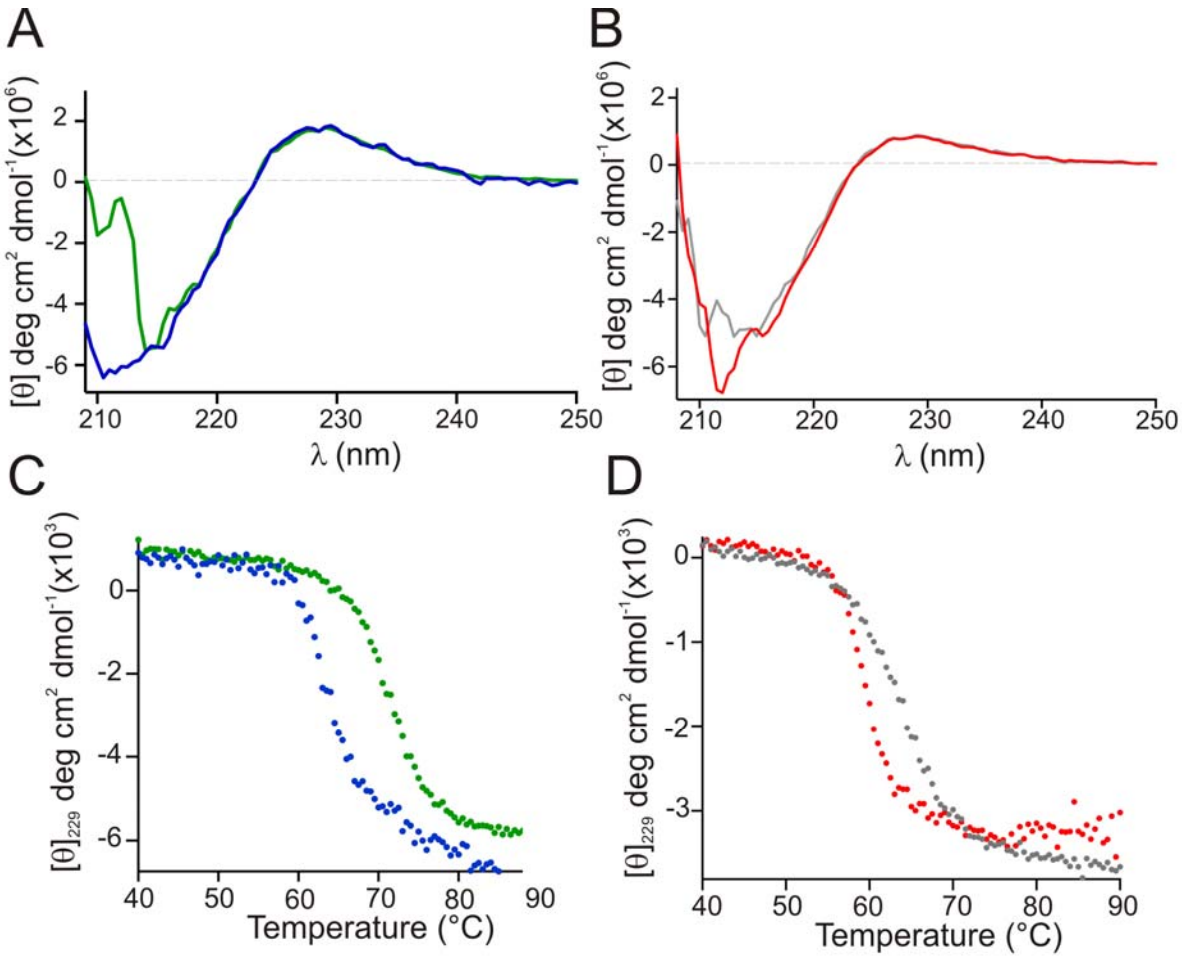

Figure S4. Related to Table 1. Thermal denaturation analysis. A) Monomeric I27wt (green) and $(I27wt)_{12}$ (blue) CD spectra at 25 ºC. **B)** Monomeric I27 Y9P (grey) and $(I27\ Y9P)_{12}$ (red) CD spectra at 25 ºC, showing (as in **A**) a typical all-β CD spectra. The color code here and in (**A**) is maintained through the rest of the figure. **C)** Thermal denaturation curves for I27wt and $(I27wt)_{12}$, as monitored by [θ] changes at 229 nm. $(I27wt)_{12}$ is less thermally stable than I27wt (**Table 1**). **D)** Thermal denaturing curve for I27Y9P and $(I27Y9P)_{12}$, as monitored by [θ] changes at 229 nm. Once again, the polyprotein is less thermally stable than the monomer.

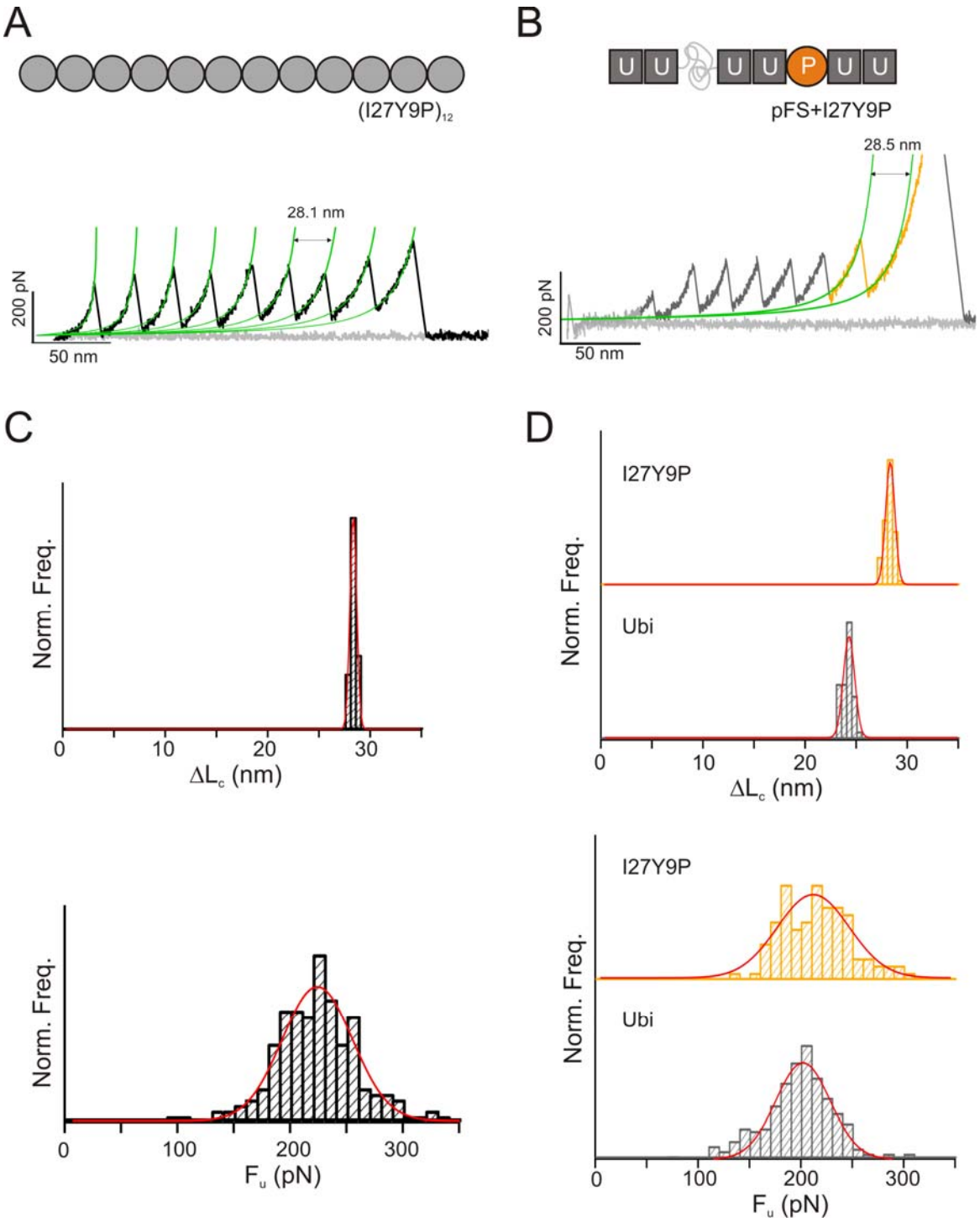

Figure S5. Related to Figures 3 and 4 and Table 1. Repetition of SMFS experiments. Since our SMFS data turned out surprising based on the values reported previously (**Figures 4, 5**; Li et al., 2000b), we repeated our experiments with I27Y9P in two different laboratories and AFMs to confirm the values reported in the main text (see **Supplemental Experimental Procedures**). Both results were comparable; here we show the ones obtained in the laboratory of Prof. Víctor Muñoz. $(I27\ Y9P)_{12}$ (**A**) and pFS+ I27Y9P (**B**) proteins were pulled in the same conditions as described in the main text. The $(I27\ Y9P)_{12}$ polyprotein (**C**) showed a ΔL_c value of 28.3 ± 0.3 nm and 222 ± 37 pN of F_u (n= 201), similar values to those reported in **Table 1** and **Figure 4**. Moreover, I27 Y9P monomer showed a ΔL_c value of 27.9 ± 0.5 nm and 216 ± 34 pN of F_u (n= 98) in the pFS+Y9P construction (**D**), similar to values reported in **Table 1**. Interestingly, the ubiquitin repeats present in pFS showed here a slightly higher F_u value (198 ± 34 pN; with 23.8 ± 0.5 nm of ΔL_c, n= 283), which could be related with the force being slightly overestimated in these measurements due to the higher noise of this apparatus. The color code in this figure corresponds to that followed in **Figures 4, 5**.

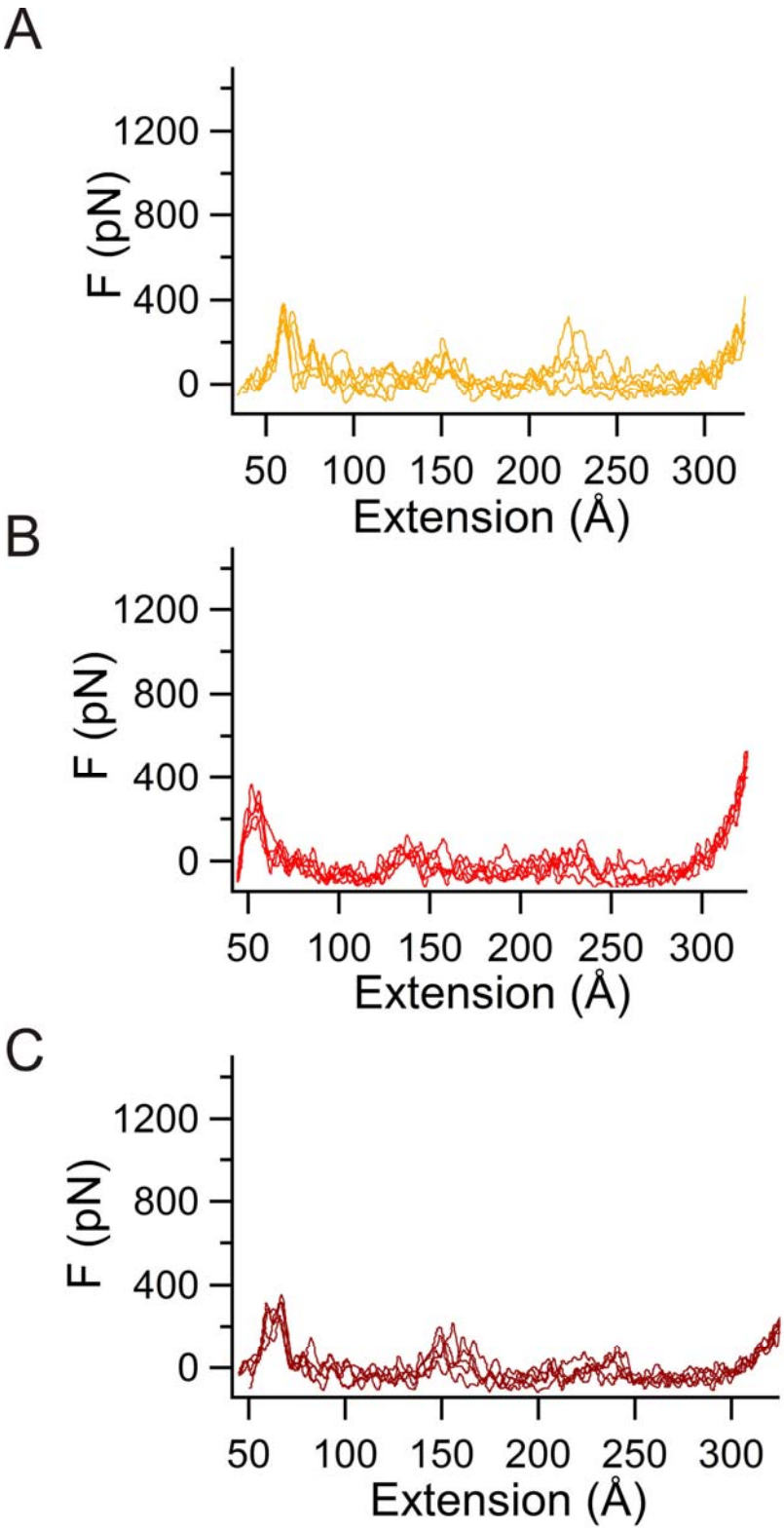

Figure S6. Related to Figure 5. Overlay of the force-extension curves obtained by SMD. All the force-extension curves obtained by SMD were plotted for I27 Y9P (PDB code 2rq8, top; Yagawa et al., 2010; **A**) and I27wt (PDB code 1tit, red; Improta et al., 1996; **B**; and PDB code 1waa, dark red; Stacklies et al., 2009; **C**). All of them show comparable force values (**Table 1**), and in the curves for I27wt, both force peaks (intermediate and main unfolding peak) can be observed (particularly in **C**, probably due to the presence of novel stabilizing interactions in N-terminus owing to the T78A mutation in 1waa, which is not present in 1tit; Stacklies et al., 2009).

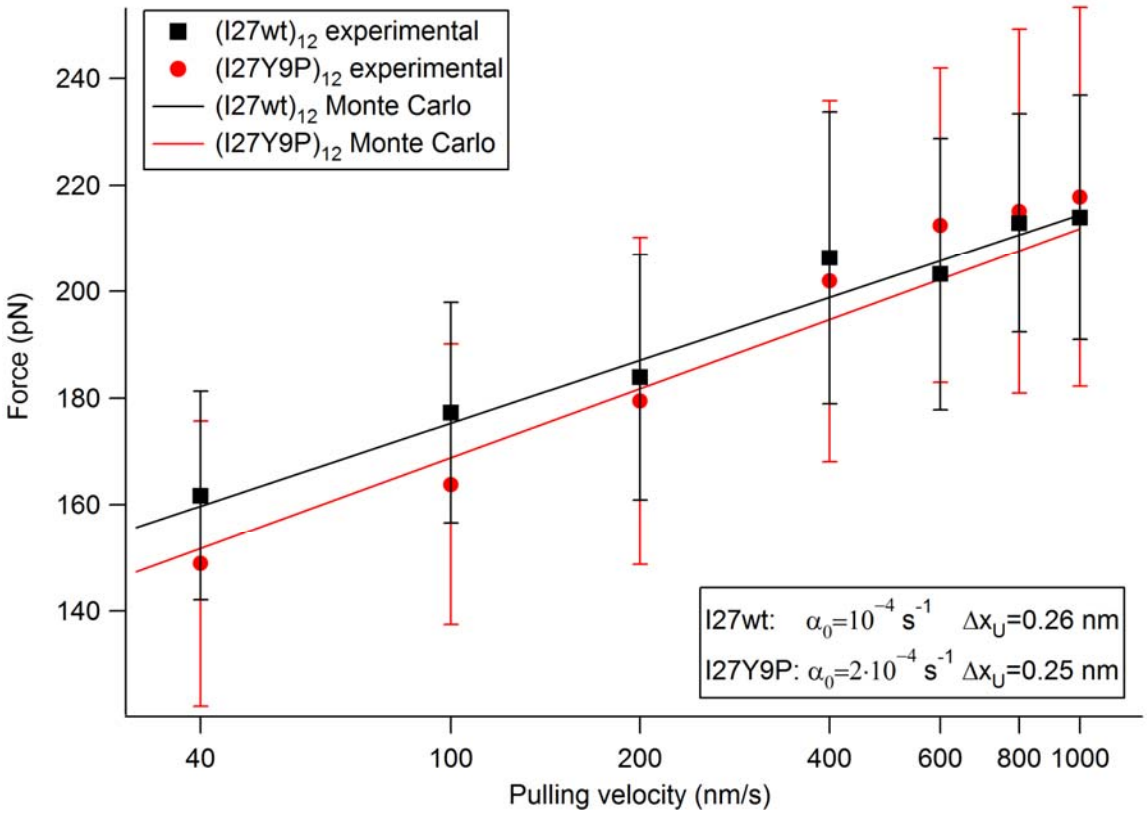

Figure S7. Related to Figures 3 and 6. Unfolding force dependence on the pulling speed for I27Y9P. The unfolding force at different pulling speeds was measured for $(I27wt)_{12}$ (black squares) and $(I27Y9P)_{12}$ (red squares). The unfolding force distributions of $(I27wt)_{12}$ and $(I27Y9P)_{12}$ were very similar at the studied pulling speeds. The kinetic parameters were estimated by performing Monte Carlo simulations of the mechanical unfolding process as previously described (Rief *et al.* 1998). The following values of α_0 and Δx_U closely reproduced the unfolding force distributions observed at the range of pulling speeds covered: I27 wt: $\alpha_0 = 10^{-4}s^{-1}$ and Δx_U 0.26 nm, I27Y9P: $\alpha_0 = 2{\cdot}10^{-4}s^{-1}$ and Δx_U 0.25 nm.

Reference	**Method**	**Sequence**	**Conditions**	**PDB file number**
Improta et al. (1996)	NMR	T42, A78	pH 4.5, 35 ºC 20 mM sodium acetate	1tit
Stacklies et al. (2009)	X-ray	A42, T78	pH 6.5, -173 ºC 20% PEG, 75 mM MES, 7.5 mM ZnSO4	1waa
Yagawa et al. (2010)	NMR	A42, T78 + Y9P	pH 7.4, 25 ºC 50 mM KPi	2rq8
This work	NMR	A42, T78 Y9 or P9	pH 4.5, 25 ºC 100 mM NaCl + 2 mM βME HX: pH 5.05 6.5 mM sodium acetate + 1 DTT	

Table S1. Related to Figure 1. Comparison of reported I27 structural studies and conditions.

Supplemental Experimental Procedures

Cloning, expression, ^{15}N-labelling and purification of the recombinant proteins

The two sequence substitutions contained in our I27wt (T42A, A78T) with respect to the 1tit sequence originally reported (Labeit and Kolmerer, 1995; deposited in ENA database; http://www.ebi.ac.uk/ena/, code CAA62188), were also present in the I27 sequence used in the pioneering SMFS experiments on titin (Rief et al., 1997). This sequence was later kept to build the I27 polyproteins (Carrión-Vázquez et al., 1999). It is unknown if these two changes represent a *bona fide* natural I27 isoform (not deposited in any database) or were the result of cloning artifacts in the original SMFS study. Indeed, the other two atomic structures described here (PDB codes 1waa and 2rq8) they both contain these changes, one of which (A78T) has been described to establish novel stabilizing interactions at the N-terminus of this module (Stacklies et al., 2009). We finally decided to maintain the described substitutions in the I27wt sequence in order to utilize identical sequences as those used in the literature to facilitate a closer comparison of the nanomechanical results. The pFS-1 vector used here is a slight modification of the sequence reported in the literature (it contains an additional N-terminal ubiquitin repeat). All the sequences (except the homomeric polyproteins) were verified by sequencing both strands of the DNA, and the cloning steps were carried out in the *E. coli* XL1-Blue strain (Stratagene). As $(I27Y9P)_{12}$ nanomechanical results were surprising to us, we decided to sequence part of this polyprotein. At least 9 out of the 12 I27Y9P repeats contained in the plasmid were sequenced and all of them were found to carry the correct mutated sequence (**Figure S1**).

The $(I27wt)_{12}$ and $(I27Y9P)_{12}$ proteins used for SMFS and thermal stability measurements were expressed in the BLR(DE3) *E. coli* strain (Novagen), while the monomer proteins used for thermal stability analyses were expressed in the BL21(DE3) strain (Novagen). Proteins based on pFS-1 were expressed in the C41(DE3) *E. coli* strain (Miroux and Walker, 1996). In all these cases, protein expression was induced for 3-4 hours by the addition of 1 mM IPTG to bacterial cultures after they reached an OD_{595} of 0.5-0.7. ^{15}N labelling for NMR of monomers and polyproteins was achieved following a previously described protocol (Marley et al., 2001) to optimize culture growth and for the incorporation of ^{15}N as $^{15}NH_4Cl$ (Cambridge Isotopes). The strain used in these cases was BL21(DE3), which showed the highest protein over-expression after IPTG induction. The incorporation of ^{15}N (97% for I27wt, 87% for I27 Y9P, ~78% for $(I27wt)_8$ was determined using MALDI-TOF-TOF Mass Spectrometry (**Figure S1**).

Bacterial pellets were lysed by treatment with 1 mg/ml lysozyme and 1% Triton X-100 (Sambrook et al., 1989). Recombinant proteins were purified by Ni^{2+}-affinity chromatography with Histrap HP (GE Healthcare) FPLC columns, using 50 mM sodium phosphate/500 mM NaCl [pH 7.4] buffer, added with 50 mM imidazole in the binding buffer and 500 mM imidazole in the elution buffer. Eluted fractions were concentrated by ultrafiltration using Amicon filters (Millipore), and they were subsequently purified by size exclusion chromatography using a Hiload 16/60 FPLC column (GE Healthcare). The buffer used in this purification step was 100 mM sodium phosphate/150 mM NaCl/1 mM DTT [pH 7.5]. Finally, purified samples were concentrated by ultrafiltration using Amicon filters and the buffer was exchanged to the appropriate one for the specific application. Protein purity was calculated to be >90% as determined by SDS-PAGE (**Figure S1**). Protein concentration was estimated by spectrophotometry using the corresponding molar extinction coefficient.

Hydrogen/Deuterium exchange by NMR spectroscopy

To further corroborate the conformation and stability of the polyproteins, we performed NMR-monitored H/D exchange experiments on $(I27wt)_8$ and $(I27Y9P)_{12}$ (**Supplemental Experimental Procedures**). These experiments should, in principle, allow us to assess whether the HN groups forming the putative backbone H-bonds show an increased resistance to exchange consistent with their bonding while HNs not participating in structural H-bonds exchange faster (Hermans et al., 1984; Huyghues-Despointes et al., 2001; Krishna et al., 2004). The corresponding protection factors (PF) and conformational free energies are shown in **Figure S3**. In the case of $(I27wt)_8$, the calculated PF values clearly show that the most protected residues are located in the secondary structures (β-strands; **Figure S3A**). $(I27Y9P)_{12}$ showed a general lower conformational thermal stability (**Figure S3B**) and the most protected regions show an arrangement comparable to the wt form. Consequently no evidences of newly formed H-bonds in $(I27Y9P)_{12}$ become apparent from H/D exchange experiments.

The exchange of amide protons with solvent deuterons was initiated by dissolving a lyophilized sample of protonated ^{15}N-(I27wt)$_8$ into deuterated solvent (6.5 mM sodium acetate/1 mM DTT). ^{15}N-(I27 Y9P)$_{12}$ showed high degradation following the aforementioned procedure. Therefore, this sample, dissolved in protonated buffer, was applied to a PD-10 gravity column (GE Healthcare) pre-equilibrated with deuterated buffer. Following elution, which exchanged the solvent protons for deuterons, the protein was concentrated using a Vivaspin filter (3 kDa cutoff, GE Healthcare). This longer processing time led to an increased exchange dead time (~130 min) and allowed more protein ^{1}H to exchange prior to the acquisition of the first NMR spectrum. These ^{1}H signals could be detected in ^{15}N-(I27wt)$_8$ due to the shorter dead time (~30 min) of the lyophilization procedure. The experimental temperature was 25 ºC, while the pH was set to 5.05 to favor exchange via the EX2 mechanism (Bruix et al., 2008). Hydrogen exchange rates were determined by integrating the volume of ^{1}H-^{15}N amide crosspeaks in a series of consecutive HSQC spectra (Bodenhausen and Ruben, 1980), using Sparky 3.114 (Goddard and Kneller). A single exponential decay function was fitted to the data to obtain the observed exchange rate, k_{ex}. In order to obtain the protection factors, PFs (*i.e.*: the ratio of the intrinsic and observed exchange rates of individual groups; k_{rc}/k_{ex}; Bai et al., 1993) of the assigned residues, k_{rc} (intrinsic exchange rates for totally denatured proteins) values were estimated based on the primary sequence, temperature and pH using the program SPHERE (http://www.fccc.edu/research/labs/roder/sphere). The conformational stability, ΔG_{HX} (**Figure S3**), of each HN group was calculated as:

$$\Delta G_{HX} = -RT\ln(k_{rc}/k_{ex}) = RT\ln PF.$$

In the case of (I27wt)$_8$, and although the exchange of the most protected HNs was incomplete under our experimental conditions (~2 days, pH 5.05, 25 ºC), the calculated PF values clearly show that the most protected residues are located in the secondary structures (β-strands) while HN in the loops and N- and C-termini exchange easily with the deuterated solvent. Interestingly, among these less protected regions, the N-terminus, residues 1-5 and 26-27, is the most stable, in accordance with the reported stabilizing effect of the nearby A78T mutation (**Figure 2F**; Stacklies et al., 2009). (I27Y9P)$_{12}$ showed lower conformational thermal stability (**Figure S4**) and the most protected regions were similar to those found in the wt form; they belong to interior H-bonding sites of β-strands. Besides, it seems that the N-terminal region of the protein (residues 1-9, 23, 26, 27, 74, 75 and 80) also shows the largest drop in protection, which would be in line with the perturbation in the mechanical intermediate suggested in the main text (**Figures 2D, E and H**).

SMFS

Before each SMFS experiment, the cantilever tip was cleaned for 1 min with a UV lamp (UV/Ozone ProCleaner™ Plus, Bioforce Nanosciences Inc.). The equipartition theorem (Florin, 1995) was used to calculate the spring constant of each cantilever with a Si_3N_4 tip (MLCT, Veeco Metrology Group; and Biolever, Olympus), which ranged from 35 to 70 pN/nm for MLCT-AUNM and was ~30 pN/nm for Biolever cantilevers. The substrate surface with the adsorbed protein sample was put in contact with the tip to pick up proteins by absorption and then withdrawn along the *z*-axis several hundred nm to stretch the proteins. Experiments were performed in the so-called length-clamp mode of SMFS (Carrión-Vázquez et al., 2006), at 0.8 nm/ms (for (I27wt)$_{12}$ and (I27 Y9P)$_{12}$) and 0.4 nm/ms both for ((I27wt)$_{12}$ and (I27 Y9P)$_{12}$) homopolyproteins as well as pFS-1+I27wt and pFS-1+I27Y9P heteropolyproteins. At least 3 experiments were performed for each protein and condition. All the data were analyzed using custom-made procedures in Igor Pro 6 (Wavemetrics). The mechanical properties of proteins were obtained by fitting the force-extension curves to the WLC model of polymer elasticity (Bustamante et al., 1994; Marko and Siggia, 1995):

$$F(x) = \frac{k_B T}{p}\left[\frac{1}{4\left(1 - x/L_C\right)^2} - \frac{1}{4} + \frac{x}{L_C}\right],$$

where F is the force, p is the persistence length, x is the end-to-end length, and L_c is the contour length of the stretched protein. L_c and p are the adjustable parameters. It should be noted that for SMFS (and in thermal stability measurements) an (I27wt)$_{12}$ construct (instead of the (I27wt)$_8$ construct used in

NMR experiments) was used to optimize the detection of the intermediate state as a deviation from the main WLC fitting (**Figure 3A**). As our NMR data indicated that the I27wt tertiary structure remains intact when inserted in a polyprotein and hence, we could use any polyprotein construction for mechanical purposes, we chose a longer polyprotein as it is reported that the unfolding intermediate species results in a gain in length of 6.6 Å per module, thus an increase which is proportional to the number of repeats (Marszalek et al., 1999). Data are reported as mean ± standard deviation. All histograms are normalized.

We have repeated the experiments with the same $(I27Y9P)_{12}$ and pFS+Y9P samples in two different laboratories and AFM set ups to confirm our SMFS data (**Figure S5**). In the laboratory of Prof. Víctor Muñoz, the experiments were performed in a PicoForce AFM equipped with a NanoScope IIIa Controller (Veeco Metrology Group), using MLCT cantilevers (Veeco Metrology Group), with a spring constant ranging from 40-50 pN/nm. Gold coverslips (Gold Arrandee™) and the same experimental conditions as those used in our laboratory were employed (namely PBS [pH 7.5] as experimental buffer and a pulling speed of 0.8 nm/ms and 0.4 nm/ms for $(I27\ Y9P)_{12}$ and pFS+I27 Y9P, respectively). Although the recordings obtained in this AFM contained higher noise levels due to an incomplete isolation, the data obtained were perfectly comparable to those described in the main text. Similar results were also obtained for these samples on a third AFM set up, in the laboratory of Prof. Andrés Oberhauser (data not shown).

The speed dependence of the F_u was done in an AFS apparatus (Luigs & Neumann) using the Olympus cantilevers with a nominal spring constant of 30 pN/nm. The measured spring constant was calculated using the method described above. The buffer and substrate were the same than those used above. The Monte Carlo simulations used were described elsewhere (Rief *et al.* 1998).

SMD

The GBSA approach used here for the SMD simulations was described elsewhere (Valbuena et al., 2009) although here the temperature was controlled using Langevin dynamics with 2 ps^{-1} as collision frequency. The SMD simulations were carried out imposing a restraint to both the N- and C-termini of the protein and increasing its length at a rate of 1 Å/ps with a constant restraint force of 5 kcal/mol·$Å^2$ (**Figure 5** and **Figure S6**). The pulling velocity of the simulations (1 Å/ ps) is about 10^8 times faster than the experimental pulling speed (0.4 nm/ ms = 4 Å/ ms $= 4 \cdot 10^{-9}$ Å / ps). Due to this difference in pulling velocities, the force values obtained in our simulations were considerably higher than those observed experimentally (**Figure 5B** and **Table 1**). All protein trajectories were visualized by VMD 1.8.6 using the structures atomic coordinates (Humphrey et al., 1996), and the N_t-C_t distance and hydrogen bond lengths (for the hydrogen bonds that constitute the mechanical clamp of the modules) were measured. We selected nitrogen and oxygen atoms that remained closer than 3.8 Å in most of the free molecular dynamics simulations, and the length of the selected backbone hydrogen bonds (with an angle cut off: < 35º) was monitored along the SMD. Forces were calculated from $C_{\alpha N\text{-}t}$-$C_{\alpha C\text{-}t}$ distance as follows:

$$F = -k\cdot[(N_t - C_t)_{measured} - (N_t - C_t)_{(0)} - v\cdot t].$$

Thermal denaturation

To assess the overall secondary structure of I27 (**Figure S4**), we monitored the I27wt, I27 Y9P, $(I27wt)_{12}$ and $(I27\ Y9P)_{12}$ far UV-CD spectra at 25 ºC in a JASCO-J810 spectropolarimeter (JASCO Inc.), equipped with a Peltier temperature control unit, using 1 mm-pathlength quartz cuvettes. The experimental buffer was 100 mM sodium phosphate/150 mM NaCl/1mM DTT [pH 7.5] and the protein concentration ranged 0.5-1 mg/ml.

The same instrument was used to monitor thermal denaturation experiments (**Figure S4**, **Table 1**). The heating rate was 0.5 ºC/min and the reversibility of the denaturation process was determined by comparing the spectra of the native proteins (before their thermally induced denaturation) with those obtained after rapidly re-cooling the heated samples. The observed changes in ellipticity (θ) at 229 nm wavelength were used to follow protein denaturation. The buffer contribution to (θ) measurements was substracted from the results that are shown. Molar ellipticity ($[\theta]$) was calculated as following (Bain et al., 2001):

$$[\theta] = \theta \cdot 100 \cdot Mr/c \cdot l \cdot Na,$$

where *Mr* is protein´s molecular weight (in Dalton), *c* is the protein concentration (in mg/ml), *l* is pathlength (in cm) and *Na* the number of residues – 1.

A model which assumes a two state folded ↔ unfolded equilibrium and linearly sloping pre- and post-transition baselines was fit to the data to obtain the parameters shown in **Table 1**.

Supplemental references

Bai, Y., Milne, J.S., Mayne, L., and Englander, S.W. (1993). Primary structure effects on peptide group hydrogen exchange. Proteins *17*, 75-86.

Bain, D.L., Berton, N., Ortega, M., Baran, J., Yang, Q., and Catalano, C.E. (2001). Biophysical characterization of the DNA binding domain of gpnu1, a viral DNA packaging protein. J. Biol. Chem. *276*, 20175-20181.

Bodenhausen, G., and Ruben, D.J. (1980). Natural abundance nitrogen-15 NMR by enhanced heteronuclear spectroscopy. J. Chem. Phys. Lett. *69*, 185-189.

Bruix, M., Ribó, M., Benito, A., Laurents, D.V., Rico, M., and Vilanova, M. (2008). Destabilizing mutations alter the hydrogen exchange mechanism in Ribonuclease A. Biophys. J. *94*, 2297-2305.

Florin, E.L., Rief, M., Lehmann, H., Ludwig, M., Dornmair, C., Moy, V.T., and Gaub, H.E. (1995). Sensing specific molecular interactions with the atomic force microscope. Biosens. Bioelectron. *10*, 895-901.

Geoghegan, K.F., Dixon, H.B., Rosner, P.J., Hoth, L.R., Lanzetti, A.J., Borzilleri, K.A., Marr, E.S., Pezzullo, L.H., Martin, L.B., LeMotte, P.K., McColl, A.S., Kamath, A.V., and Stroh, J.G. (1999). Spontaneous alpha-N-6-phosphogluconoylation of a "His tag" in Escherichia coli: the cause of extra mass of 258 or 178 Da in fusion proteins. Anal. Biochem. *267*, 169-184.

Hermans, J., Berendsen, H.J.C., Van Gunsteren, W.F., and Postma, J.R.M. (1984). A consistent empirical potential for water-protein interactions. Biopolymers *23*, 1513-1518.

Humphrey, W., Dalke, A., and Schulten, K. (1996). VMD: Visual Molecular Dynamics. J. Mol. Graph. *14*, 33-38.

Huyghues-Despointes, B.M., Pace, C.N., Englander, S.W., and Scholtz, J.M. (2001). Measuring the conformational stability of a protein by hydrogen exchange. Methods Mol. Biol. *168*, 69-92.

Krishna, M.M., Hoang, L., Lin, Y., and Englander, S.W. (2004). Hydrogen exchange methods to study protein folding. Methods *34*, 51-64.

Marley, J., Lu, M., and Bracken, C. (2001). A method for efficient isotopic labelling of recombinant proteins. J. Biomol. NMR *20*, 71-75.

Miroux, B., and Walker, J.E. (1996). Over-production of proteins in *Escherichia coli*: mutant hosts that allow synthesis of some membrane proteins and globular proteins at high levels. J. Mol. Biol. *260*, 289-298.

Rief, M., Gautel, M., Schemmel, A. and Gaub, H. (1998). The mechanical stability of immunoglobulin and fibronectin III domains in the muscle protein titin by atomic force microscopy. Biophys. J. *75*, 3008-3014.

Sambrook, J., Fritsch, E.F., and Maniatis, T. (1989). Molecular Cloning: A Laboratory Manual, 2nd Ed (New York: Cold Spring Harbor).